

# The reactive transport of Li as a monitor of weathering processes in kinetically limited weathering regimes

Madeleine S. Bohlin\*, Mike J. Bickle

Dept. Earth Sciences, University of Cambridge, Downing Street, Cambridge CB2 3EQ, UK.

## ARTICLE INFO

### Article history:

Received 9 October 2018  
Received in revised form 11 January 2019  
Accepted 19 January 2019  
Editor: D. Vance

### Keywords:

Lithium  
Li isotopes  
Chemical weathering  
Himalayas  
Reactive transport

## ABSTRACT

Analytical solutions to reactive-transport equations describing the evolution of Li concentrations and isotopic ratios are presented for one-dimensional flow paths where reaction stoichiometry is constant along the flow path. These solutions are considered appropriate for chemical weathering in rapidly eroding catchments. The solutions may be described by two dimensionless numbers; 1) a Damköhler number describing the product of reaction rate and fluid residence time, and 2) a net partition coefficient which describes the fraction of Li re-precipitated in secondary minerals as the product of a fluid-secondary mineral partition coefficient and the mass fraction of secondary mineral precipitates. In settings where water entering flow paths is dilute, Li concentrations will increase along the flow path until they reach a limiting value determined by the net partition coefficient. Simultaneously,  $^7\text{Li}/^6\text{Li}$  isotopic ratios will increase to a limiting value of the source rock ratio minus the secondary mineral-fluid Li-isotopic fractionation factor. Waters with Li-isotopic ratios in excess of this limiting value must have evolved with a change of reaction stoichiometry and/or partition coefficient along the flow path such that at some point net removal of Li to secondary minerals exceeds that supplied by dissolution of primary minerals. The modelling shows that the multiple controls on chemical weathering rates (temperature, rainfall, erosion rate, hydrology) cannot be inferred from Li concentration and isotopic ratio data alone, which only provide two independent constraints. Caution should be exercised in interpretation of oceanic Li records in terms of potential climatic variables. The model is illustrated by a set of Li concentration and isotopic ratio measurements on river waters and bed sands in the Alaknanda river basin which forms the headwaters of the Ganges. This illustrates how values of the Damköhler number and net partition coefficient can be used to trace weathering processes. Water samples from catchments with similar lithologies and climates scatter along contours of approximately constant net partition coefficient, reflecting similar reaction stoichiometries, but with more variable Damköhler numbers reflecting variations in flow path length, fluid flux and/or reaction rate. Samples from the lower, warmer and less rapidly eroding catchments have high  $^7\text{Li}/^6\text{Li}$  isotopic ratios with lower Li concentrations and must reflect at least a two-stage weathering process where reaction stoichiometry and/or Li fluid-mineral partition coefficients change along the flow path so that net Li is removed in the later stages.

## 1. Introduction

Chemical weathering of silicate rock is thought to provide the negative feedback that maintains the equable climate on Earth (Berner et al., 1983; Chamberlin, 1899; Walker et al., 1981). However the nature and magnitude of the climatic and tectonic controls on riverine solute fluxes are uncertain and thus their roles in moderating long-term global climate are disputed (Bluth and Kump, 1994; Maher and Chamberlain, 2014; West et al., 2005). In part this reflects the potential complexities of the bed-rock, climatic and tectonic controls and in part the difficulty of distinguishing the silicate chemical weathering inputs from the much larger inputs from weathering of carbonate rocks.

Lithium concentration and isotopic compositions are a promising proxy for silicate weathering processes as dissolved Li is almost entirely derived from the dissolution of silicate minerals (Kisakürek et al., 2005; Millot et al., 2010b). The weathering systematics of Li are relatively simple with negligible biological cycling (Lemarchand et al., 2010; Pogge von Strandmann et al., 2016) and congruent primary mineral dissolution (Pistiner and Henderson, 2003; Verney-Carron et al., 2011; Wimpenny et al., 2010). Importantly, the formation of secondary mineral phases such as clays or oxy-hydroxides preferentially incorporates  $^6\text{Li}$  (Vigier et al., 2008) which fractionates the Li isotopic composition and generates continental reservoirs with significantly different Li isotopic compositions (Dellinger et al., 2015; Huh et al., 1998; Kisakürek et al., 2005).

Riverine Li-isotopic compositions are often modelled by zero-dimensional batch- or Rayleigh models (Bouchez et al., 2013; Dellinger et al., 2017; Dellinger et al., 2015; Kisakürek et al., 2005). However, these models do not properly reproduce the results of reactive transport

\*Corresponding author.

E-mail address: [madeleine.bohlin@gmail.com](mailto:madeleine.bohlin@gmail.com)

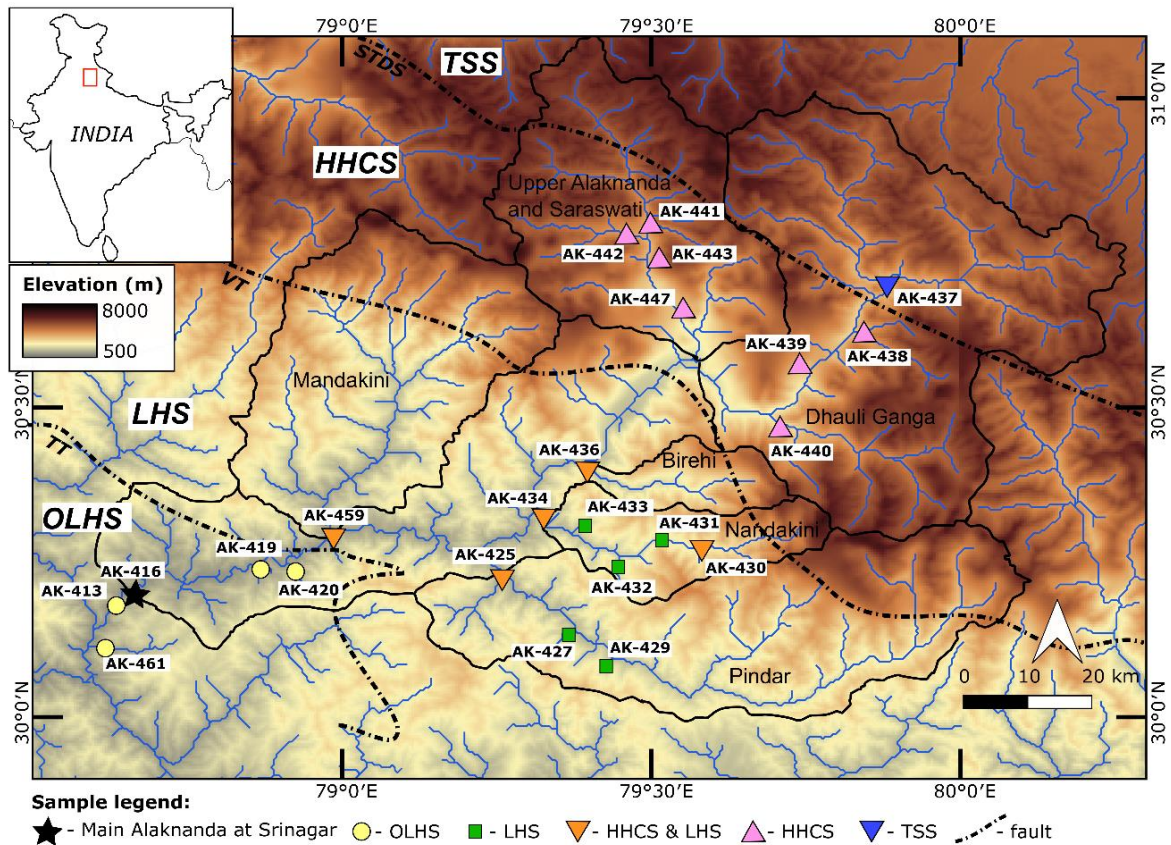


**Figure 1.** Map of the Alaknanda river basin with subdivision of lithotectonic units. TSS = Tibetan Sedimentary Series, HHCS = High Himalayan Crystalline Series, LHS = Lesser Himalayan Series, OLHS = Outer Lesser Himalayan Series, STDS = South Tibetan Detachment system, VT = Vaikrita Thrust, TT = Tons Thrust. The terrain is coloured based on elevation which ranges from ~450 meters to ~7800 meters within the catchment. Digital Elevation Model downloaded from USGS HydroSHEDS 15 sec SRTM data.

in natural environments in which water flows through porous soils, sapprolite and rock with Li being continuously supplied by dissolution reactions, removed by precipitation reactions and advected by the fluid flow.

Silicate weathering is more suitably modelled by reactive transport equations which describe flow and reaction in a porous medium (Fontorbe et al., 2013; Maher, 2010, 2011; Maher and Chamberlain, 2014). Models based on numerical thermodynamic codes which couple the complete descriptions of the mineral reactions with transport have previously been developed and applied to the Li isotopic system (Liu et al., 2015; Wanner et al., 2017; Wanner et al., 2014). However, the complexity of such models may obscure the key controlling processes. Simpler analytical solutions have also been presented where either the ratio of Li precipitation in secondary minerals to that supplied by dissolution is held constant (Lemarchand et al., 2010) or where the rate of Li partitioning into secondary minerals is described by a constant partition coefficient (Pogge von Strandmann et al., 2014). In this paper we present similar analytical solutions to a one-dimensional reactive transport model adapted from that of Fontorbe et al. (2013) previously applied to silicon isotopic variations in Himalayan and Gangetic floodplain rivers. The approach allows determination of the impacts of the various climatic and tectonic controls on chemical weathering and riverine Li systematics. The model shows that the evolution of Li concentrations and isotopic compositions in kinetically limited weathering regimes may be described by only two dimensionless

numbers, in addition to the choice of starting and boundary conditions, and the clay mineral-fluid Li-isotopic fractionation factor.

This paper describes the modelling, and the implications of the modelling, illustrated by Li concentration and isotopic compositions of a set of river water and sediment samples from the kinetically limited weathering regime in the Alaknanda river basin in the Himalayan mountains. Weathering in ‘kinetically-limited’ environments provides the feedback that moderates climate on long timescales (e.g. West et al., 2005) and the objective is to use Li-isotope systematics to help elucidate these climatic controls on silicate weathering. We also discuss the evolution of Li systematics in the Ganges flood plain based on previously published Li-isotopic analyses (Bagard et al., 2015; Huh et al., 1998; Manaka et al., 2017; Pogge von Strandmann et al., 2017).

## 2. The Headwaters of the Ganges in the Himalayan Mountains

The high exhumation rates coupled to the orographic monsoon system make the Himalayas and the Ganges-Brahmaputra river system one of the largest transport systems of solutes and sediments to the oceans (Gaillardet et al., 1999; Huh, 2010; Milliman and Meade, 1983). River chemistry in the headwaters of the Ganges has been subject to numerous studies (e.g. Bickle et al., 2003; Bickle et al., 2005; Bickle et al., 2001; Bickle et al., 2015; Chakrapani and Saini, 2009; Singh and Hasnain, 1998). Here, we use the Li concentration and isotopic composition of the dissolved load and bed sands of the Alaknanda river basin (NW India) to illustrate the reactive transport model developed

below. The Alaknanda river basin may be divided into four physiographic regions of contrasting geology (Fig. 1). These comprise 1) the largely unmetamorphosed siliciclastic and carbonaceous sedimentary rocks of the Tibetan Sedimentary Series (TSS), 2) the high-grade gneisses, schists and granites of the High Himalayan Crystalline Series (HHCS), 3) the low- to medium grade schists, phyllites and massive dolomites of the Lesser Himalayan Series (LHS) and 4) the low grade metasediments of the Outer Lesser Himalayan Series (OLHS) at the most southern part of the basin. Although confined within a kinetically limited weathering regime, the weathering characteristics are expected to vary across the basin due to the large range in erosion rates and climate, and contrasts in lithologies.

The Himalayan catchments sampled for this study range from 4 to 11000 km<sup>2</sup> (Fig. 1, for their location, area, and physiographic details see Supplementary material Table A1). They cross an extreme range of climatic and vegetation zones. The TSS is mainly exposed on the Tibetan plateau above 3000 m where there are permanent ice sheets, vegetation is sparse, agriculture is very restricted and precipitation is limited (~270 mm/yr) (Bookhagen and Burbank, 2010). The HHCS extends from altitudes above 1000 m to nearly 8000 m. Vegetation ranges from pine forests and Alpine meadows to rocky and ice covered mountain tops and rainfall ranges from 600 to 900 mm/yr with ~45% occurring during the monsoon season. The OLHS and LHS extend from altitudes of a few hundred meters to ~3700 m; these catchments are often densely forested (oaks, alder, rhododendron) with significant terracing for agriculture in limited areas. The climate ranges from subtropical at the lowest altitudes to Alpine on the highest peaks and precipitation ranges between ~1500 and 2700 mm/yr, with 75% occurring during the monsoon season. Erosion rates range from  $0.8 \pm 0.3$  mm/yr in the LHS,  $1.2 \pm 0.1$  mm/yr in the TSS to  $2.7 \pm 0.3$  mm/yr in the HHCS (Vance et al., 2003).

The water and bed sand samples analysed were collected in October 2014 from small catchments with restricted lithological and climatic parameters as well as larger catchments. The sampling and analytical procedures are detailed in Supplementary material Appendix A. The major cation and anion compositions (Supplementary material Table A2) lie in the range of samples reported previously from these catchments (e.g. Bickle et al., 2003, 2005, 2015) and are bicarbonate-dominated with high Ca reflecting inputs from carbonate lithologies (Bickle et al., 2005; Bickle et al., 2015). Average total dissolved solids are high in the TSS (176 mg/L), lowest in the HHCS (average 76 mg/L) and increase through the LHS (98 mg/L) and OLHS (140 mg/L) but show much scatter related to controls by lithology, climate and catchment size.

## 2.1 Li concentrations and isotopic compositions of river waters and bed sands in the Alaknanda river basin

Analytical procedures for Li-isotopic ratios followed Bohlin et al. (2018). The contribution of atmospheric and hydrothermal input to the Li budget is small (Supplementary material, Appendix B).

Dissolved Li concentrations in the Alaknanda basin range from 58 to 2362 nmol/l (Supplementary material Table A3). The rivers draining the TSS and HHCS have the highest dissolved Li concentrations despite having total dissolved solid loads (TDS) lower than those in the LHS and OLHS (Supplementary material Table A2). Li concentrations of bed sands (Supplementary material Table A3) range from 17 to 384 ppm with the highest values in the HHCS probably derived from

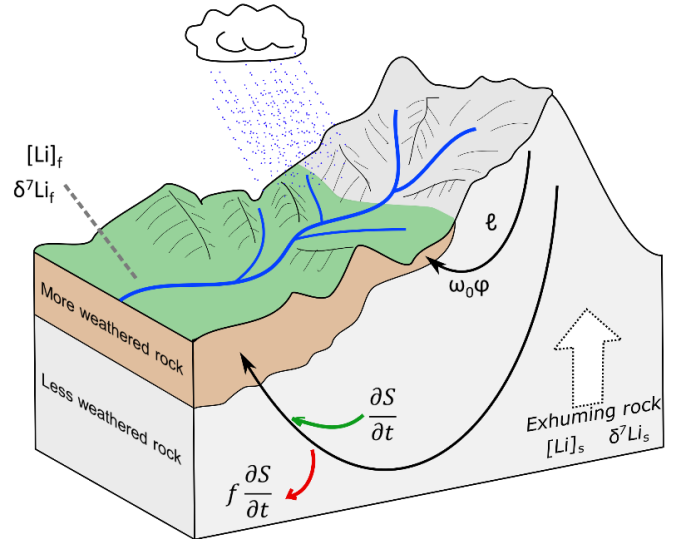


**Figure 2.** A schematic representation of the one-dimensional reactive transport model. River waters consist of mixtures of shallow and deep subsurface flow paths where water flows with an advective flux  $\omega_0\phi$ , along the flow path length  $l$ . The rock is exhumed much more slowly through the weathering zone such that shallower flow paths will tend to be through more altered rock. The Li concentration and isotopic compositions of waters are a function of the dissolution rate  $\frac{\partial S}{\partial t}$  and the rate of removal of Li from precipitation of secondary clays  $f\frac{\partial S}{\partial t}$ .

pegmatites associated with leucogranites which outcrop close to the South Tibetan Detachment System.

The  $\delta^7\text{Li}$  composition of the dissolved load ranges from +7.4 to +35.3‰ with the highest values found in rivers draining the LHS and OLHS (Supplementary material Table A3). There is a large range in river bed sand  $\delta^7\text{Li}$  (-3.3 to +10‰) reflecting bed-rock heterogeneity. TSS, HHCS and OLHS bed sediments are characterised by negative  $\delta^7\text{Li}$  compositions (-3.3 to 0.7‰) whereas the LHS sediments are almost exclusively positive (-0.6 to 10.0‰, Supplementary material Table A3). The two samples with bed sand  $\delta^7\text{Li} > +3\%$  (AK425 and AK427) are from the LHS Pindar catchment which includes outcrops of the volcanic-bearing Rautgara and Nagthat-Berina formations (Valdiya, 1980).  $\delta^7\text{Li}$  in modern basalts altered by seawater may reach values as high as +14‰ (Chan et al., 1992). The apparent fractionation between waters and bed sediments ( $\Delta^7\text{Li}_{f-s}$ , where  $\Delta^7\text{Li}_{f-s} = \delta^7\text{Li}_f - \delta^7\text{Li}_s$ ) is systematically lower in rivers draining the TSS and the HHCS and increases from 8.1‰ to 32.2‰ towards the OLHS in the south of the catchment.

The marked fractionation of Li-isotopic compositions in the waters ( $\delta^7\text{Li}$  between 8 and 35‰) from the source rock compositions (mean  $0.1 \pm 1.7\%$ ,  $1\sigma$  excluding the two bed sand samples with high  $\delta^7\text{Li}$ ) is ascribed to precipitation of clay minerals which have significant fluid-mineral Li-isotopic fractionation factors (Huh et al., 1998). Interpretation of the changes in Li concentrations and isotopic compositions requires a model of both how the fluid interacts with the bed rock minerals and the nature of the fluid-mineral reactions and reaction products. Below we formulate a simple reactive transport model in a form that allows interpretation of the Li systematics and how these might relate to the controlling climatic and tectonic variables.

### 3. Model framework: One-dimensional reactive transport model for the weathering environment

#### 3.1 Assumptions and model framework

The simplifying assumptions in our modelling are appropriate to chemical weathering in rapidly eroding mountain belts. In such environments the weathering takes place along flow paths which range from near surface to depths of kilometres, the deepest supplying the meteoric water-dominated hot springs (Becker et al., 2008; Coussens et al., 2018; Evans et al., 2001). The time-varying chemistries of river waters attest to input from groundwater systems with varying residence times and weathering characteristics (Calmels et al., 2011; Tipper et al., 2006). The hysteresis between precipitation and river discharge implies average groundwater residence times of  $\sim 45$  days in equivalent Himalayan catchments in Nepal and that  $2/3^{\text{rds}}$  of the river discharge passes through the groundwater system which is in relatively low porosity fractured rock (Andermann et al., 2012). Mineral weathering in the river channel is minimal in the fast flowing mountain rivers (Bickle et al., 2005). The weathering system thus comprises waters flowing at a wide range of rates through flow paths with a range of lengths, depths and through rock with variable alteration states. These waters may mix in the groundwater flow system and are finally all mixed in the rivers with the potential for additional dilution by precipitation or enrichment by evapo-transpiration. The rock is exhumed much more slowly through the weathering zone such that shallower flow paths will tend to be through more altered rock (Figure 2). In the rapidly eroding mountains, the fraction of silicate minerals weathered (weathering intensity) is characteristically small. For example, in the Himalayan mountains only  $\sim 2\%$  of the mass of the soluble silicate load is dissolved (e.g. Bickle et al., 2015). However, the weathering intensity is likely to be heterogeneous with much of the groundwater flow confined to fractured rock localising alteration to fracture walls. In the higher mountains accumulations of glacial moraine and landslide debris may weather more homogeneously (Emberson et al., 2016) and in the lower catchments in the Himalayas there is significant development of soils, although erosion is still

dominated by landslides which preclude the development of mature soil weathering profiles.

It is not possible to derive a full hydrological and mineralogical description of the weathering systems in rapidly eroding terrains because neither the hydrological nor the geological structure can be sampled with the necessary resolution. To evaluate the possible responses of such systems to climatic and tectonic controls we initially model the simplest component of the hydrological system; reaction in a one-dimensional flow path along which the silicate mineral reaction stoichiometry and reaction rate are constant. The limited extent of silicate mineral dissolution in ‘kinetically limited’ weathering regimes makes this an appropriate approximation. This contrasts with weathering of mature soil profiles in which a series of mineral reaction fronts can be mapped migrating downwards (e.g. Maher et al., 2009; White et al., 2008). The model presented here allows the consequences of the main potential controls on weathering systematics to be evaluated. These include the impacts of temperature and rainfall (fluid flux), and reaction progress which is controlled by mineralogy, reaction rate and time. Time is ultimately a function of erosion rate. The consequences of more complex weathering systems, where source rock composition and reaction stoichiometry vary along the flow path and fluids from flow paths with differing characteristics mix, may then be approximated by considering the riverine compositions as the sum of outputs from a set of such flow paths or mixing from different flow paths. We show that it is not possible to infer the impact of dilution or concentration of solutes by considering the relationship between Li isotopic ratios and element ratios (e.g. Li/Na) although this does allow comparison of their respective Damköhler numbers and thus the relative dissolution rates between Li- and Na-bearing minerals.

#### 3.2 A model for Li concentration and isotopic ratios

The evolution of the Li concentration ( $L_i$ ) and isotopic composition ( $\delta^7Li_i$ ) of the fluid with respect to time ( $t$ ) and distance ( $z$ ) along a one-dimensional flow path, may be described by

**Table 1**

Definitions and units of variables used in the reactive transport model

Variable	Definition	Units
$\varphi$	Porosity of medium	$\text{m}^3 \cdot \text{m}^{-3}$
$\omega_0$	Flow velocity of fluid	$\text{m} \cdot \text{s}^{-1}$
$\omega_0 \varphi$	Fluid flux	$\text{m} \cdot \text{s}^{-1}$
$L_i, L_s, L_c$	Li concentration of fluid (f), solid (s), clay (c)	$\text{mol} \cdot \text{m}^{-3}$
$\delta^7Li_f, \delta^7Li_{f,0}, \Delta^7Li_{f-s}, \delta^7Li_s, \delta^7Li_c$	Li isotopic composition of fluid (f), initial fluid (f,0), fluid relative to solid (f-s), solid (s), clay (c)	$\text{‰}$
$\Delta$	Fractionation factor ( $\delta^7Li_c - \delta^7Li_f$ )	$\text{‰}$
$K_v$	Volumetric partition coefficient of Li between fluid and clay minerals	
$t, t_e$	Time ( $t$ ), time rock is weathered before eroded ( $t_e$ )	s
$z$	Distance along flow path	m
$\ell$	Flow path length	m
$Li', Na', t', z'$	Dimensionless variables for concentrations ( $Li'$ ) and ( $Na'$ ), time ( $t'$ ) and distance ( $z'$ )	
$S$	Volume fraction of silicate rock weathered	
$\partial S / \partial t$	Reaction rate of silicate rock	$\text{s}^{-1}$
$f$	Volume fraction of dissolved rock precipitating as secondary minerals	
$N_D^{Li}$	Damköhler number for Li	
$N_D^{Na}$	Damköhler number for Na	
$K_{net}$	Net partition coefficient for Li ( $f \cdot K_v$ )	

$$\varphi \frac{\partial Li_f}{\partial t} = -\omega_0 \varphi \frac{\partial Li_f}{\partial z} + \frac{\partial S}{\partial t} Li_s - f \frac{\partial S}{\partial t} K_v Li_f \quad (1)$$

and

$$\begin{aligned} \varphi \frac{\partial Li_f \delta^7 Li_f}{\partial t} = & -\omega_0 \varphi \frac{\partial Li_f \delta^7 Li_f}{\partial z} + \frac{\partial S}{\partial t} Li_s \delta^7 Li_s \\ & - f \frac{\partial S}{\partial t} K_v Li_f (\delta^7 Li_f + \Delta) \end{aligned} \quad (2)$$

where  $\varphi$  is the porosity of the rock or soil ( $m^3 \cdot m^{-3}$ ),  $\omega_0$  is the flow velocity of the fluid ( $m \cdot s^{-1}$ ), and  $\omega_0 \varphi$  is thus the water flux ( $m \cdot s^{-1}$  or  $m^3 \cdot m^{-2} \cdot s^{-1}$ ).  $\partial S / \partial t$  is the reaction rate at which a volume fraction of silicate rock,  $S$ , is being chemically weathered with time,  $t$ , ( $s^{-1}$ ), with a concentration  $Li_s$  ( $mol \cdot m^{-3}$ ) (variables defined in Table 1). Therefore,  $\partial S / \partial t \cdot Li_s$  is the reaction rate at which lithium bearing rocks weather and release Li into the fluid ( $mol \cdot m^{-3} \cdot s^{-1}$ ), with an isotopic composition  $\delta^7 Li_s$  (‰). A volume fraction  $f$  of chemically weathered rock is reprecipitated as clay minerals, having a Li concentration  $Li_c$  ( $mol \cdot m^{-3}$ ). It is assumed that the concentration of Li in the clay minerals may be related to that of the fluid by a volumetric partition coefficient,  $K_v$ , where

$$K_v = \frac{Li_c}{Li_f} \quad (3)$$

and its isotopic composition is related to the fluid by the fractionation factor  $\Delta$  (‰), where  $\Delta = \delta^7 Li_c - \delta^7 Li_f$ .

It is convenient to convert equations (1) and (2) to non-dimensional time, distance and fluid-concentration variables,  $t'$ ,  $z'$  and  $Li'$  related to the fluid flow path length  $\ell$ , fluid flux  $\omega_0 \varphi$ , and the concentration of Li in the primary silicate rock,  $Li_s$ . The following transformations

$$\begin{aligned} z &= z' \ell \\ t &= \frac{\ell}{\omega_0 \varphi} t' \end{aligned} \quad (4)$$

$$Li_f = Li' Li_s$$

allow equations (1) and (2) to be re-written as

$$\varphi \frac{\partial Li'}{\partial t'} = - \frac{\partial Li'}{\partial z'} + N_D^{Li} (1 - K_{net} Li') \quad (5)$$

$$\begin{aligned} \varphi \frac{\partial Li' \delta^7 Li_f}{\partial t'} = & - \frac{\partial Li' \delta^7 Li_f}{\partial z'} \\ & + N_D^{Li} [\delta^7 Li_s - K_{net} Li' (\delta^7 Li_f + \Delta)] \end{aligned} \quad (6)$$

in terms of two dimensionless constants

$$N_D^{Li} = \frac{\partial S}{\partial t'} \quad (7)$$

$$K_{net} = f K_v \quad (8)$$

$N_D^{Li}$  is a Damköhler number (c.f. Bickle, 1992; Lassey and Blattner, 1988; Maher, 2010) and  $K_{net}$  is a net volumetric fluid-mineral Li partition coefficient which also takes into account the fraction of clay minerals formed. These transformations identify the minimum independent variables and account for variations in bedrock Li concentrations.

Because  $\varphi$  is small ( $1 - \varphi \approx 1$ ), the left hand sides of equations (5) and (6) are negligible except on short timescales (quasi-stationary state approximation; (Lichtner, 1988) and the equations may be simplified to

$$\frac{\partial Li'}{\partial z'} = N_D^{Li} (1 - K_{net} Li') \quad (9)$$

$$\frac{\partial Li' \delta^7 Li_f}{\partial z'} = N_D^{Li} [\delta^7 Li_s - K_{net} Li' (\delta^7 Li_f + \Delta)] \quad (10)$$

If the supply of Li from rock dissolution is greater than the removal from clay precipitation then  $K_{net} Li' < 1$  (which in terms of equation 1 is expressed as  $\frac{\partial S}{\partial t} Li_s > f \frac{\partial S}{\partial t} K_v Li_f$ ) and if the removal is greater than the supply then  $K_{net} Li' > 1$ .

If the rate of rock dissolution ( $\partial S / \partial t$ ) is assumed constant along the flow path, the solutions to equations (9) and (10) are

$$Li' = \frac{1}{K_{net}} - \left( \frac{1}{K_{net}} - Li'_0 \right) e^{-N_D^{Li} K_{net} z'} \quad (11)$$

and

$$\begin{aligned} \delta^7 Li_f &= \frac{e^{N_D^{Li} K_{net} z'} (\delta^7 Li_s - \Delta) + N_D^{Li} K_{net} (1 - K_{net} Li'_0) z' \Delta + C}{e^{N_D^{Li} K_{net} z'} - (1 - K_{net} Li'_0)} \end{aligned} \quad (12)$$

where  $Li'_0$  is the initial dimensionless concentration of Li in the fluid and  $C$  is the constant of integration.  $C$  is calculated from the boundary condition at  $z'=0$ , where the isotopic composition of the fluid is  $\delta^7 Li_{f,0}$ , which gives

$$C = \delta^7 Li_{f,0} K_{net} Li'_0 - \delta^7 Li_s + \Delta \quad (13)$$

Equations 11 and 12 are essentially identical to equations A6 and A7 in Pogge von Strandmann et al. (2014) except for the approximations inherent in using  $\delta$  values.

$K_{net}$  and  $N_D^{Li}$  may be calculated from sample Li concentrations and isotopic compositions, given values for the initial Li concentration and isotopic composition at  $z'=0$ , by solving equations 11 and 12 to give expressions for  $K_{net}$  in terms only of  $Li'$  and  $\delta^7 Li$

$$\begin{aligned} \delta^7 Li_f \left( \frac{1 - Li'_0 K_{net}}{1 - Li' K_{net}} \right) - \delta^7 Li_f + \delta^7 Li_f Li'_0 K_{net} - \\ \left( \frac{1 - Li'_0 K_{net}}{1 - Li' K_{net}} \right) (\delta^7 Li_s - \Delta) - \Delta \ln \left( \frac{1 - Li'_0 K_{net}}{1 - Li' K_{net}} \right) + \\ Li'_0 K_{net} \Delta \ln \left( \frac{1 - Li'_0 K_{net}}{1 - Li' K_{net}} \right) - \delta^7 Li_{f,0} Li'_0 K_{net} + (\delta^7 Li_s - \\ \Delta) = 0 \end{aligned} \quad (14)$$

Equation 14 has two roots, however only the positive root is physically plausible. Given  $K_{net}$  from the solution of equation 14, the Damköhler number may then be calculated using equation 11.

### 3.3 Modelling Li isotopic ratios versus Li/Na ratios

The evolution of the fluid Na concentration ( $Na_f$ ) may be modelled by a similar equation to that for Li (equation 1) except that Na is not partitioned into structural sites on secondary minerals (ie  $f_{Na}=0$ ). We ignore the possibility of significant Na on exchangeable sites. Thus

$$\varphi \frac{\partial Na_f}{\partial t} = -\omega_0 \varphi \frac{\partial Na_f}{\partial z} + \frac{\partial S}{\partial t} Na_s \quad (15)$$

Making the stationary-state assumption (i.e.  $\frac{\partial Na_f}{\partial t} = 0$ ), and transforming time, distance by equations 4 and Na concentrations by

$$Na_f = Na' Na_s \quad (16)$$

where  $Na_s$  is the Na concentration of bedrock gives the non-dimensional evolution of Na with distance along flow paths as

$$\frac{\partial Na'}{\partial z'} = N_D^{Na} \quad (17)$$

For the boundary condition  $Na' = Na'_0$  at  $z'=0$ , the solution to equation 17 is

$$Na' = N_D^{Na} \cdot z' + Na'_0 \quad (18)$$

Therefore, combining equations 11 and 17 for the condition  $Li' = Li'_0$  at  $z'=0$ , gives the variation of dimensionless Li/Na ratio ( $Li'_n$ ) as

$$Li'_n = \frac{Li'}{Na'} = \frac{(1 - (1 - K_{net} \cdot Li'_0) e^{-N_D^{Li} \cdot K_{net} \cdot z'})}{K_{net} (N_D^{Na} \cdot z' + Na'_0)} \quad (19)$$

Since Li isotopic compositions are functions only of  $N_D^{Li} \cdot K_{net}$  (given  $\Delta$  and taking  $z'=1$ ), Li/Na ratios provide information on the ratio of  $N_D^{Li}$  to  $N_D^{Na}$ . However it is not possible to derive values of  $K_{net}$  or  $N_D^{Li}$  from the relationship between  $\delta^7Li$  and Li/Na and avoid the secondary effects of dilution or evaporative concentration, as discussed below.

#### 4. Implications

Equations 11 and 12 imply that the evolution of the concentration of Li and its isotopic composition along a fluid flow path is only dependent on the distance along the fluid flow path,  $z'$ , and two dimensionless variables; the net partition coefficient of Li between the fluid and forming secondary minerals,  $K_{net}$ , and the Damköhler number,  $N_D^{Li}$ , given the clay mineral-fluid isotopic fractionation factor  $\Delta$ . Since the flow path length,  $\ell$ , is used as the scaling length in equation 4,  $z'$  equals 1 at the end of the flow path. The significance of  $N_D^{Li}$  and  $K_{net}$  is discussed below.

##### 4.1 The net partition coefficient of Li, $K_{net}$ , and the Damköhler number, $N_D^{Li}$

The net partition coefficient of Li in the weathering environment,  $K_{net}$  (eq 8), describes the magnitude of Li uptake into the precipitating clay minerals as a function of the fluid Li concentration. It depends on the volume fraction of dissolved rock which is reprecipitated as clay minerals ( $f$ ), and a volumetric partition coefficient of Li between the clay minerals and water ( $K_v$ ). The  $f$ -factor is dependent solely on the stoichiometry of the weathering reaction. For weathering of siliceous crustal rocks,  $f$  generally increases as reactions progress from feldspar dissolution to minerals with higher Al/Si ratios, and as the product smectite/kaolinite ratio increases as Al is essentially insoluble (Supplementary material Appendix C). Few studies have been made on clay mineral Li partition coefficients at ambient temperatures, but they are likely to vary with temperature, aqueous chemistry and mineral type (Vigier et al., 2008; Decarreau et al., 2012). Empirical relationships derived from laboratory experimental data (Decarreau et al., 2012)

yield values of  $K_v$  in the order of  $10^3$  to  $10^6$  for typical surface waters (Supplementary material Appendix D).

The Damköhler number,  $N_D^{Li}$ , is given by equation 7 as

$$N_D^{Li} = \frac{\partial S}{\partial t'} = \frac{\partial S}{\partial t} \frac{\ell}{\omega_0 \varphi} \quad (20)$$

where  $N_D^{Li}$  depends on the rate of rock dissolution ( $\partial S/\partial t$ ), the fluid flow path length ( $\ell$ ) and the advective water flux ( $\omega_0 \varphi$ ). Note that the term  $\ell/\omega_0 \varphi$  relates to the fluid residence time ( $\ell/\omega_0$ ). Because the Damköhler number is the product of reaction rate, path length and water flux it is not possible to use Li concentrations and their isotopic ratios alone to determine the individual impacts of these parameters on the weathering system without additional catchment specific information.

##### 4.2 Li concentration and isotopic evolution along flow paths

The variation of Li concentration and isotopic composition with distance along the flow path is illustrated in Fig. 3 for two examples. In the first case, more Li is supplied to the fluid through dissolution than is being removed by clay mineral formation, i.e.  $K_{net} \cdot Li' < 1$ . Li concentrations and isotopic ratios both increase along the flow path. The Li concentration increases towards a limiting value at which supply and removal balance ( $K_{net} \cdot Li' = 1$ ), a value that is inversely proportional to  $K_{net}$ . The fluid Li-isotopic composition,  $\delta^7Li_f$ , approaches  $\delta^7Li_s - \Delta$  when  $K_{net} \cdot N_D^{Li} \geq 5$  (note the solid-fluid fractionation factor,  $\Delta$ , is negative). For the second case, removal of Li from clay precipitation is greater than the supply, i.e.  $K_{net} \cdot Li' > 1$ . The example simulates a change in reaction stoichiometry for an input fluid that had reached steady-state Li and  $\delta^7Li_f$  compositions with  $\Delta = -17\%$ . Li concentrations decrease with distance, but the isotopic composition initially increases and then subsequently decreases approaching  $\delta^7Li_s - \Delta$  when  $K_{net} \cdot N_D^{Li} \geq 10$ . The decrease in  $\delta^7Li_f$  occurs when fluid Li concentrations are sufficiently low that addition of Li from continued dissolution (of rock with lower  $\delta^7Li$ ) starts to dominate the dissolved Li pool. If  $K_{net} \cdot Li' > 1$ , the fluid  $\delta^7Li_f$  may increase to much higher values than the offset of the fractionation factor, approaching Rayleigh fractionation as  $K_{net}$  becomes very large.

The combined control of  $K_{net}$  and  $N_D^{Li}$  on Li concentrations and isotopic compositions is explored in Fig. 4. If  $K_{net} \cdot Li' < 1$ , for a given value of  $K_{net}$ , faster dissolution rates and/or longer fluid residence times (higher Damköhler number  $N_D^{Li}$ ) result in both higher Li concentrations and  $\delta^7Li_f$  at any given point in the flow path (Fig. 4a, b) until these reach the limiting steady state values. If  $K_{net} \cdot Li' > 1$ , which requires the initial fluid to have a significant Li concentration, coupled higher values of  $K_{net}$  and  $N_D^{Li}$  lead to faster removal of Li and an increase in the maximum Li isotopic composition attained (Figs. 4c, d).

##### 4.3 Coupled dissolution and precipitation: the reactive transport grid

A plot of bedrock-normalised fluid Li-isotopic composition ( $\Delta^7Li_{f-s}$ ) against dimensionless Li concentration ( $Li'$ ) may be contoured with values of  $K_{net}$  and  $N_D^{Li}$  calculated from equations 11 and 14 (Fig. 5). This calculation requires assumption of the initial Li concentration and isotopic composition of the input fluid, the Li isotopic fractionation factor  $\Delta$ , and scales distance to the flow path length ( $z'=1$ ). It illustrates the various possible pathways in which waters may evolve to the sampled river composition. Two grids of  $K_{net}$  and  $N_D^{Li}$  contours are shown on Fig. 5. The lower grid assumes input waters are dilute (i.e.  $Li'_0=0$ ) and simulates the first stage of chemical weathering with rainwater input to a flow path with constant reaction stoichiometry and

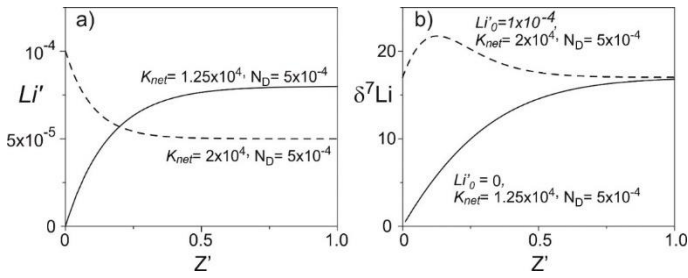


**Figure 3.** Illustration of variation of Li concentration and isotopic composition with distance along a flow path (equations 11 and 12) for a Li-isotopic fractionation factor,  $\Delta = -17\%$ . a) Shows concentration with solid line calculated for an initial concentration of 0 ( $Li'_0 = 0$ ) and dashed line calculated for  $Li'_0 = 1 \times 10^{-4}$ . Note increase in  $K_{net}$  for second case is reflected in lower steady-state Li concentration. b) Solid line takes  $Li'_0 = 0$  and shows monotonic increase in Li-isotopic ratio. Dashed line takes  $Li'_0 = 1 \times 10^{-4}$  and initial fluid  $\delta^7Li_f = 17\%$  and shows increase in  $\delta^7Li$  to a maximum value and then decrease to a steady state value of  $+17\%$  (dashed line) given assumed secondary mineral–fluid fractionation of  $-17\%$  and rock  $\delta^7Li = 0\%$ . The Damköhler number is scaled to the length of the flow path.

rate and the clay mineral–fluid isotopic fractionation factor,  $\Delta = -17\%$  (see below for discussion of fractionation factors). For such a weathering scenario both fluid Li concentrations and isotopic compositions are limited to maximum values,  $Li' \leq 1/K_{net}$  and  $\delta^7Li_f \leq \delta^7Li_s - \Delta$  (i.e.  $\Delta^7Li_{f-s} \leq -\Delta$ ) (Fig. 2). If  $K_{net} \cdot Li' > 1$ , possible only if the input waters have significant Li,  $\delta^7Li_f$  will increase and then decrease along the flow path as Li concentrations decrease. This is illustrated by the upper grid on Fig. 5, which is drawn for assumed initial values of  $\delta^7Li_{f,0}$  ( $17\%$ ) and  $Li'_0$  ( $2.53 \times 10^{-5}$ ) as discussed below.

In the reactive transport grid (Fig. 5), contours of  $K_{net}$  represent constant mineral reaction stoichiometries. At the earliest stages of weathering, dilute rain water entering the flow path will acquire initial Li-isotopic compositions close to the composition of the rock. At the low weathering intensities expected in rapidly eroding Himalayan catchments, the waters would be expected to evolve along the flow path with a near constant mineral reaction stoichiometry (i.e. along the  $K_{net}$  contours in the lower part of fig. 5) with increasing Li concentrations and  $\delta^7Li$  ratios until a steady state is approached ( $N_D^{Li}$  exceeding  $10^{-5}$  to  $10^{-3}$  for  $K_{net}$  varying from  $10^6$  to  $10^4$ ). The increase is mapped by  $N_D^{Li}$  of which higher values reflect some combination of faster reaction rates, longer flow path lengths or smaller fluid fluxes. The  $\delta^7Li$  of the water can only increase above the steady state Li-isotopic value of  $\delta^7Li_s - \Delta$  if there is a change in reaction stoichiometry and/or partition coefficient so that  $K_{net} \cdot Li'$  exceeds 1. If so, more Li is removed from solution than is being supplied from dissolution and the grid changes structure with the waters decreasing in Li concentrations and initially increasing to higher  $\delta^7Li$  values before returning to equilibrium with the unreacted rock (Figs. 3, 4). Again, higher values of  $N_D^{Li}$  are reflected by the more rapid return of  $\delta^7Li$  towards equilibrium.

#### 4.4 Complications: Mixing, dilution and evaporative enrichment of fluids

Mixing of fluids from separate flow paths, changes in reaction stoichiometry/partition coefficient ( $K_{net}$ ) and dilution or enrichment by addition of rain or evapo-transpiration of emerging groundwaters may complicate interpretations. If, as expected, a range of groundwater flow paths in a small catchment have similar  $K_{net}$  values but a range of path lengths and fluid fluxes, mixtures of two such fluids will lie on a

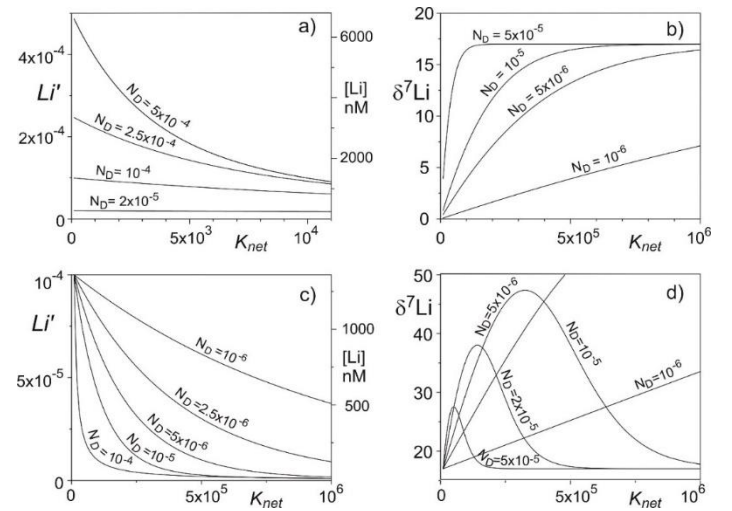


**Figure 4.** The effect of varying Damköhler number  $N_D^{Li}$  and net partition coefficient  $K_{net}$ . Dissolved Li concentration and isotopic composition plotted against  $K_{net}$  with contours of varying  $N_D^{Li}$ . Note that increasing Damköhler number is equivalent to increasing path length and/or increasing rock dissolution rate. In (a) and (b) more Li is being supplied to the water through dissolution than being removed through clay precipitation ( $K_{net} \cdot Li' < 1$ ) and the starting composition  $Li'_0$  of the water at the beginning of the flow path is 0. In (c) and (d) more Li is removed than supplied ( $K_{net} \cdot Li' > 1$ ) and  $Li'_0$  is taken as  $1 \times 10^{-4}$  and  $\delta^7Li_{f,0}$  as  $17\%$ . The concentrations on the right-hand axes of Figs 3a and c are scaled to a solid ( $Li_s$ ) concentration of 35 ppm (average crust of Teng et al., 2004) and the isotopic evolution in Figs 3b and d takes  $\delta^7Li_s = 0\%$  and the secondary mineral–fluid fractionation factor ( $\Delta$ ) as  $-17\%$ .

concave mixing hyperbola above the convex  $K_{net}$  contour and plot at an apparent Damköhler number that is some weighted average of the flow paths. Mixing from flow paths with different  $K_{net}$  values with or without different Damköhler numbers would take place along hyperbolic mixing curves crossing  $K_{net}$  contours. If the value of  $K_{net}$  changed part way along a flow path,  $Li'$  and  $\Delta^7Li_{f-s}$  would map a trajectory across to the new  $K_{net}$  contour. Although analysis of single samples would contain no information on such mixing or changes in  $K_{net}$ , the scatter of sets of samples from tributaries in smaller catchments might be expected to reflect the range in  $N_D^{Li}$ , systematic changes in  $K_{net}$  and the nature of the mixing in water leaving the catchments.

Dilution or enrichment of waters prior to entering groundwater flow paths is unlikely to be important as Li concentrations are likely to be low. Significant enrichment or dilution of waters at the end of flow paths would result in samples being displaced parallel to the  $x$ -axis on the reactive transport grid causing either an increase in apparent  $K_{net}$  and a decrease in apparent Damköhler number with dilution or the opposite for evaporative enrichment. Plotting a reactive transport diagram comprising  $\Delta^7Li_{f-s}$  versus  $Li'/Na'$  does not reveal information about the impact of such changes in concentration on  $N_D^{Li}$  and  $K_{net}$  as equations 12 and 19 collapse onto a single curve (Fig. 6) where  $\Delta^7Li_{f-s}$  increases with the product  $K_{net} \cdot N_D^{Li}$ . The intercept, if  $Li'_0$  and  $Na'_0$  are small, is equal to  $N_D^{Li}/N_D^{Na}$ , providing information on the relative dissolution rates of Li and Na bearing minerals.

#### 5 Li-isotope systematics of the Alaknanda catchments: Calculation of $N_D$ and $K_{net}$

The model discussed above shows how the Li-isotope systematics may be discussed in terms of the dimensionless constants  $N_D^{Li}$  and  $K_{net}$

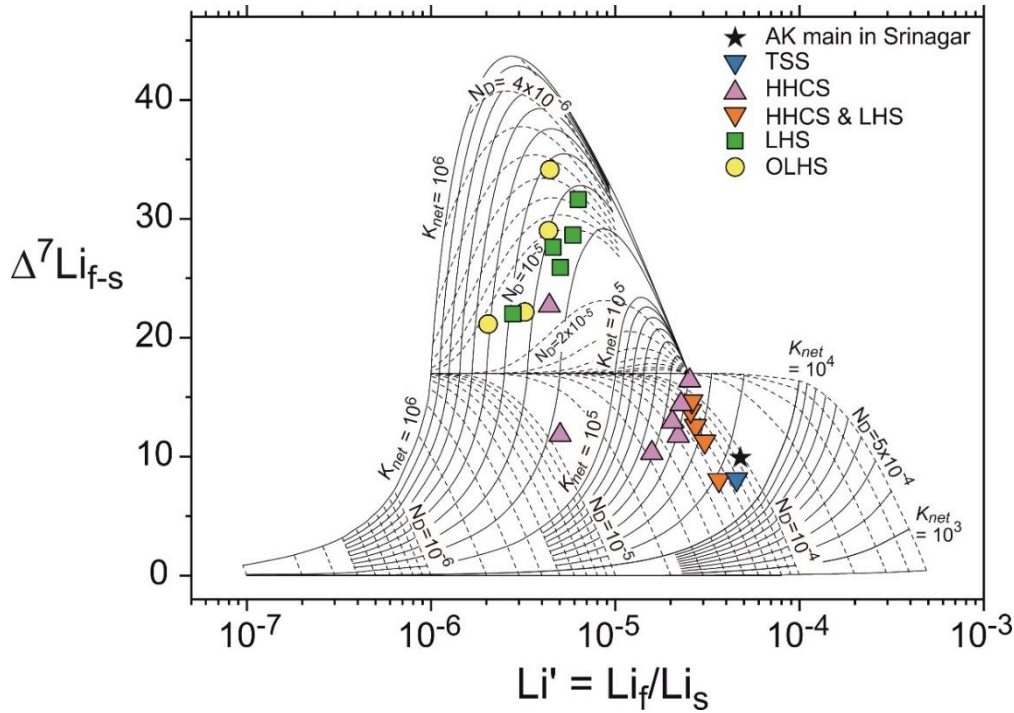


**Figure 5.** A grid mapping evolution of dimensionless Li concentration ( $Li' = Li_f/Li_s$ ) and isotopic compositions ( $\Delta^7Li_{f-s} = \delta^7Li_f - \delta^7Li_s$ ) of waters for ranges of values of the Damköhler number ( $N_D^{Li}$ ) and net partition coefficient ( $K_{net}$ ). The lower grid ( $\Delta^7Li_{f-s} < 17$ ) is calculated for  $Li'_0 = 0$  and therefore  $K_{net}Li' < 1$  where more Li is supplied from dissolution than being removed from clay precipitation, and the upper grid with initial conditions  $Li'_0 = 2.53 \times 10^{-5}$ , and  $\delta^7Li_f = 17\text{‰}$  for  $K_{net}$  values which give  $K_{net}Li' > 1$  so that more Li is removed than supplied. Solid lines of the grid are contours of  $K_{net}$  and dashed lines are contours of  $N_D^{Li}$ . At low weathering intensities waters are expected to evolve along lines of constant  $K_{net}$  reflecting near constant reaction stoichiometry and fluid-secondary mineral partition. Isotopic compositions in the upper grid ( $\Delta^7Li_{f-s} > 17$ ) can only be accessed if reaction stoichiometry and/or Li partition coefficient change so that  $K_{net}Li' > 1$ . Analyses of samples from the Himalayan catchments are plotted with  $Li'$  scaled to bedload Li concentration and  $\Delta^7Li_{f-s}$  calculated taking  $\delta^7Li_s$  equal to the bedload Li-isotopic composition (see text Section 4.2). The initial Li concentration for the upper grid is taken by extrapolating the average  $K_{net}$  of the HHCS samples to  $\delta^7Li_f = 17\text{‰}$ .

given a value for the clay mineral-water Li-isotopic fraction factor,  $\Delta$ . We evaluate the constraints on the magnitude of  $\Delta$  below. Calculation of  $N_D^{Li}$  and  $K_{net}$  for an individual water sample is based on the Li concentration and isotopic composition of both the dissolved load and bed rock from equations 12 and 14, in conjunction with assumption of their initial values at the beginning of the flow path ( $Li'_0$  and  $\delta^7Li_{f,0}$ ) as discussed below. Bed sands are used as a proxy for the bedrock, as bed sands in the Himalayas are minimally weathered and provide a catchment integrated rock composition.

### 5.1 Estimates of the clay-water Li-isotopic fractionation factor ( $\Delta$ )

Mineral-fluid Li-isotopic fractionations are likely to vary with temperature, mineral species, precipitation rates and fluid compositions. In weathering of Himalayan silicate crust product minerals containing significant Li are likely to include kaolinite, smectites, chlorite, Fe-oxyhydroxides, vermiculite and other alteration products of biotite. There are few direct constraints on clay mineral-fluid Li-isotopic fractionation factors. Vigier et al. (2008) synthesised smectites (Li-rich hectorites) and extrapolate isotopic fractionation factors for Li in structural sites measured between 250 °C and 90 °C to imply  $\Delta^7Li \sim -17$  to  $-19\text{‰}$  at temperatures between 20 and 5 °C. Experiments at temperatures below 90 °C were thought not to be in equilibrium. They found Li on exchangeable sites exhibited very small fractionations, consistent with experiments by Pistiner and Henderson (2003) on both smectites and Fe-oxyhydroxides. Zhang et al. (1998) calculated fractionation factors from Li-uptake into vermiculite,

kaolinite and a Mississippi River clay recalculated as  $\Delta^7Li = -31, -18$  and  $-21\text{‰}$  with uncertainties of  $\sim 5\text{‰}$ . Millot et al. (2010a) derived fractionation factors from seawater-basalt experiments between 25 and 250 °C which imply  $\Delta^7Li \sim -19\text{‰}$  at surface temperatures from a best fit regression against  $1/T$  (K).

There have been a number of attempts to use natural fractionations to recover the underlying fractionation factors. Chan et al. (1992) analysed ocean floor basalts altered at low temperatures and interpreted their Li-isotopic compositions to reflect mixing between pristine basalt and secondary clays with a fractionation factor against seawater (2 °C) of  $\sim -19\text{‰}$ . Other studies have modelled Li-isotopic variations in river and groundwaters against Li or Li/Na ratios with both batch and Rayleigh fractionation and recovered fractionation factors between  $\sim -5$  to  $-25\text{‰}$  (Bagard et al., 2015; Dellinger et al., 2015; Lemarchand et al., 2010; Pogge von Strandmann et al., 2017). The problem with this approach is that weathering along flow paths with reactive transport can produce similar trends but these deviate from Rayleigh or batch fractionation trends. We discuss possible further constraints on clay mineral-fluid Li-isotopic fraction factors from the Himalayan data below.

### 5.2 $N_D^{Li}$ and $K_{net}$ and the transition in weathering processes across the Alaknanda Basin

The Himalayan data divides into two groups on the  $\Delta^7Li_{f-s} - Li'$  diagram (Fig. 5). Nearly all the TSS, HHCS and HHCS+LHS rivers have  $\Delta^7Li_{f-s} < 17\text{‰}$ ,  $Li'$  between  $5 \times 10^{-6}$  and  $5 \times 10^{-5}$  and  $K_{net} < 6 \times 10^4$ .



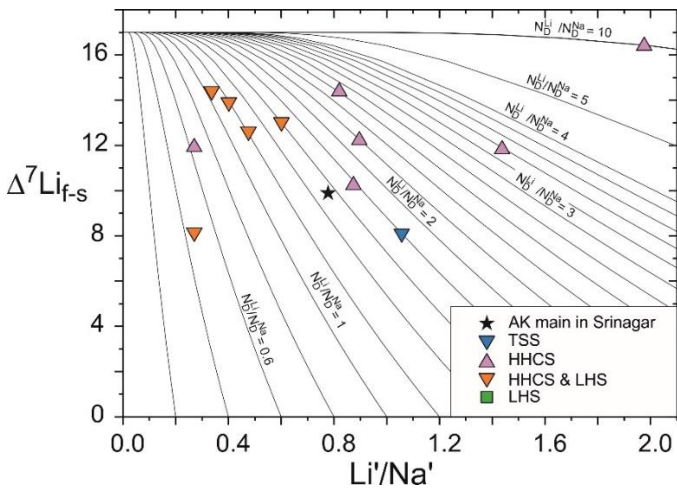


**Figure 6.**  $\Delta^7\text{Li}_{f-s}$  to  $\text{Li}'/\text{Na}'$  of Alaknanda water samples with contours representing  $N_D^{Li}/N_D^{Na}$ . Note that dilution or evaporative enrichment of waters does not change sample locations as the product  $N_D^{Li} \cdot K_{net}$  and the ratio  $\text{Li}'/\text{Na}'$  remain constant. Note most samples plot within a factor of 2 of  $N_D^{Li}/N_D^{Na} = 1$ .

The LHS and OLHS rivers have  $\Delta^7\text{Li}_{f-s} \geq 21\%$ ,  $\text{Li}' < 6.6 \times 10^{-6}$  and  $K_{net} > 2 \times 10^5$ . The coincidence of high  $\Delta^7\text{Li}_{f-s}$  with lower  $\text{Li}'$  of the LHS and OLHS samples is taken to indicate that these samples evolved with a stage of decreasing  $\text{Li}'$  with  $K_{net} \cdot \text{Li}' > 1$ . This requires that their waters underwent a minimum of two stages of reactive transport. The first stage from rainwater necessarily elevated both  $\text{Li}'$  and  $\delta^7\text{Li}_f$ . The second followed an increase in  $K_{net}$ , which reduced  $\text{Li}'$ , but further increased  $\delta^7\text{Li}_f$ . The division between the low and high  $K_{net}$  groups occurs at values of  $\Delta^7\text{Li}_{f-s}$  between  $\sim 17$  and  $21\%$  which lies in the range of the best estimates of  $\Delta$  (Chan et al., 1992; Millot et al., 2010a; Vigier et al., 2008). A clay mineral–fluid fractionation factor in the range  $20 \pm 3\%$  is also consistent with field studies that note fluid  $\delta^7\text{Li}_{f-s}$  is largely capped in this range. These include the other major study of river waters in the Himalayas (Kisakürek et al., 2005), the Ganges mainstem in the flood plain where  $\Delta^7\text{Li}_{f-s}$  rises to  $\sim 22\%$  and nearly all the tributaries are less than  $23\%$  (Pogge von Strandmann et al., 2017) and the Strengbach catchment where  $\Delta^7\text{Li}_{f-s}$  in streams and springs ranges up to  $19.3\%$  (Lemarchand et al., 2010) (see Supplementary material Appendix F, Figs. F1, F3).

Where  $\Delta^7\text{Li}_{f-s}$  exceeds  $\sim 23\%$  there is some evidence of two stage processes. For example, in the Strengbach catchment soil water Li concentrations initially increase with depth before a marked decrease between 30 and 60 cm, associated with a large increase in  $\delta^7\text{Li}$  (Lemarchand et al., 2010).

On Fig. 5 the input fluid composition for the upper grid is taken as close to the composition of the most evolved HHCS samples on the lower grid ( $\Delta^7\text{Li}_{f-s} = 17\%$  and  $\text{Li}' = 2.53 \times 10^{-5}$ ). The minimum initial  $\text{Li}'$  must be greater than  $1.24 \times 10^{-5}$  for a reaction-precipitation mechanism to produce the sample with the most extreme  $\text{Li}'$  and  $\Delta^7\text{Li}_{f-s}$  (AK429). Assumption of  $\text{Li}'_0 = 1.24 \times 10^{-5}$  makes little difference to calculated second stage  $K_{net}$  and  $N_D^{Li}$  values (changing the mean  $K_{net}$  for the LHS and OLHS samples from  $3.2 \times 10^5 \pm 8 \times 10^4$  to  $4.3 \times 10^5 \pm 1.1 \times 10^5$ , 2se,  $n=7$ ), excluding the two samples with the highest  $\text{Li}'$  and  $\Delta^7\text{Li}_{f-s}$  values. Likewise decreasing  $\Delta$  to  $-21\%$  and increasing the input Li-isotopic composition ( $\delta^7\text{Li}_{f,0}$ ) to  $21\%$  only decreases the mean  $K_{net}$  to  $2.8 \times 10^5 \pm 7 \times 10^4$  and increases the mean  $N_D^{Li}$  from  $1.2 \times 10^{-5} \pm 1.5 \times 10^{-6}$  to  $1.8 \times 10^{-5} \pm 1.9 \times 10^{-6}$  (2se,  $n=9$ ).

The catchments in the Alaknanda basin cluster around three values of  $K_{net}$  (Fig. 5). The lowest values average at  $1.7 \times 10^4 \pm 2 \times 10^3$  (2se,  $n=3$ ). These samples represent the earliest stages of weathering within the basin including the output from the TSS, the Birehi river in the LHS and the mainstream Alaknanda at its outlet in Srinagar. The high Li flux of the latter indicates that the Li flux exiting the Himalayan mountains is predominantly sourced from incipient weathering reactions in the upper parts of the Ganga headwaters. A majority of the sampled HHCS rivers and the mainstem tributaries that drain the HHCS and LHS are characterised by intermediate values of  $K_{net}$  (mean  $4.1 \times 10^4 \pm 5.3 \times 10^3$  2se,  $n=9$ ). The highest values of  $K_{net}$  are calculated for the second stage of weathering in the tributaries draining the LHS and OLHS (mean  $3.1 \times 10^5 \pm 6.5 \times 10^4$  2se,  $n=9$ , Supplementary material Table E1).

The distinct  $K_{net}$  values thus reveal three dominant weathering regimes within the basin. Within these regimes the spread in  $\Delta^7\text{Li}_{f-s}$  and  $\text{Li}'$  may be explained by variations in the Damköhler number. Values of  $N_D^{Li}$  are generally highest in larger catchments, presumed to result from longer fluid flow paths and residence times. Dilution of groundwater inputs to rivers by dilute surface runoff would decrease the values estimated for  $N_D^{Li}$  and increase the estimates for  $K_{net}$ . The consistency of the  $K_{net}$  values within  $\pm 35\%$  in the HHCS grouping suggests that, if dilution is significant across these very different size catchments, it varies remarkably little. The much larger proportional spread in  $N_D^{Li}$  (140% about the mean) is consistent with the main control on the weathering progress being hydrological and some combination of fluid flux, flow path length and possibly reaction rate. The more complicated weathering regime in the LHS and OLHS, with a second stage characterised by high  $K_{net}$ , is plausibly related to the slower erosion rate and warmer climate which allow increased reaction progress in nearer surface rocks sampled along the later parts of hydrological flow paths. However, the role of lithological differences may also be significant.

### 5.3 Comparison with other Himalayan and the Strengbach catchments

The  $\text{Li}'$  and  $\Delta^7\text{Li}_{f-s}$  values of rivers sampled by Kisakürek et al. (2005) in the Nepal Himalayas show a similar distribution to the Alaknanda samples (Supplementary material, Fig. F1). The TSS samples scatter to the lowest values of  $K_{net}$  ( $10^4$ ) and highest values of  $N_D^{Li}$  ( $5 \times 10^{-4}$ ) similar to the Alaknanda TSS sample. Most of the HHCS samples show a wider scatter but are centred on the Alaknanda HHCS samples. The wide scatter likely reflects seasonal variations, as samples from Kisakürek et al. (2005) were collected in both the pre- and post-monsoon seasons when hydrological conditions are markedly different, in combination with the broader geographic spread of these samples. Eight of the eleven HHCS samples from the Dudh Khosi (south of Mt Everest), have a distinct composition with  $\Delta^7\text{Li}_{f-s}$  between 18 and  $23\%$  and  $\text{Li}' < 2 \times 10^{-6}$ . The LHS samples from Nepal have similar compositions to the HHCS samples, unlike those from the Alaknanda catchments. These samples were taken from small catchments along an 8 km stretch of the Bhoti Kosi and presumably represent less advanced weathering than the Alaknanda LHS samples.

The Strengbach catchment drains a small catchment underlain by an altered leucogranite in the Vosges Mountains. Streams and springs exhibit a range of  $\Delta^7\text{Li}_{f-s}$  from 6 to  $19\%$  and  $\text{Li}'$  mostly less than  $3 \times 10^{-6}$  (Lemarchand et al., 2010) (Supplementary material Fig. F1). Again,  $\Delta^7\text{Li}_{f-s}$  is limited to  $\leq 19\%$ , consistent with a single stage of weathering with the most evolved waters close to steady-state.

#### 5.4 Comparison of $N_D^{Li}$ and $N_D^{Na}$

Fig. 6 illustrates the distribution of the Alaknanda samples on the  $\Delta^7Li_{f-s}$  to Li'/Na' reactive transport grid. The majority of the samples lie between  $0.6 < N_D^{Li}/N_D^{Na} < 2.2$  (mean 1.6). Provided the rain and spring-corrected Na concentrations reflect plagioclase dissolution, the  $N_D^{Li}/N_D^{Na}$  ratios imply that dissolution of micas, which are likely to contain more Li than feldspars, is comparable to that of plagioclase. This difference is well within the scatter of estimates of feldspar and biotite dissolution rates compiled by White and Brantley (2003).

#### 5.5 Weathering in the Ganges floodplain

The Li-isotopic compositions in the Ganga mainstem rise rapidly from ~12‰ at the mountain front to ~20‰ 500 km downstream and then remain within the range 19-24‰ (except one dry season value of 27‰) for the rest of the river course (Bagard et al., 2015; Huh et al., 1998; Manaka et al., 2017; Pogge von Strandmann et al., 2017), (Supplementary material, Figs F2, F3). The Yamuna, tributaries that rise on the floodplain, major tributaries from the north that rise in the Himalayas (except the Gandak, 16.7‰) and those from the south from the basalts of the Deccan plateau have  $\Delta^7Li_r$  in the range 19-24.8‰. Thirteen of the sixteen tributaries have  $\delta^7Li_r$  in the range  $20 \pm 1\%$ . This indicates that weathering on the floodplain occurs at Damköhler numbers sufficient to reach steady-state with  $\Delta^7Li_{f-s} = -\Delta$ . It should be noted that 'steady-state' Li-isotopic compositions do not imply weathering is supply-limited. The shallow groundwaters (< 40 m) with  $\delta^7Li_r$  up to 30‰ (Bagard et al., 2015) imply that weathering in some aquifers reached the second stage where  $Li' \cdot K_{net} > 1$ , unless the fractionation factor,  $\Delta$ , was much more negative than indicated by experiments. A floodplain groundwater contribution may explain the higher  $\delta^7Li_r$  ratios in the mainstem and some tributaries (although the average shallow groundwater  $\delta^7Li_r$  is ~22‰). Lupker et al. (2012) and Bickle et al. (2018) estimated that weathering on the floodplain contributes about 50% of the silicate-derived chemical fluxes discharged by the Ganges, and the limited Li concentration data implies a similar fractional input for Li.

#### 6. Constraints on climatic and tectonic controls from $N_D^{Li}$ and $K_{net}$

Previous discussions of riverine Li-isotopic ratios have mostly been based on zero-dimensional batch or Rayleigh fractionation models (e.g. Bouchez et al., 2013; Dellinger et al., 2015; Misra and Froelich, 2012), and interpreted in terms of 'weathering intensity' defined as the ratio of chemical denudation rate to the total denudation rate. For the assumptions made here, applicable to rapidly eroding environments, the  $\delta^7Li$  of the dissolved load is controlled by the several parameters which comprise the Damköhler number ( $N_D^{Li}$ ) and the net partition coefficient ( $K_{net}$ ) but not simply by the 'weathering intensity'. Water discharged from a flow path has a constant  $\delta^7Li$  ratio while the stoichiometry of the weathering reactions and Li mineral-fluid partition coefficients remain unchanged. The  $\delta^7Li$  of the eroded material is determined by the ratio of the solid weathering products ( $t_e \cdot \partial S / \partial t$  where  $t_e$  is the duration of the weathering) to residual unweathered rock ( $1 - t_e \cdot \partial S / \partial t$ ) and the  $\delta^7Li$  of the weathering products. The latter is given by the integral of the Li-isotopic composition of the weathering products over the path length (i.e.  $(\int_0^l \delta^7Li_c dz) / l$  where  $l$  is path length and  $\delta^7Li_c$  is the  $\delta^7Li$

**Table 2**

Impact of changes (increases) in climatic and tectonic variables on  $N_D^{Li}$  and  $K_{net}$

	$\partial S / \partial t$	$\omega_0 \phi$	$\frac{\ell}{\omega_0 \phi}$	$S$	$N_D^{Li}$	$K_{net}$
Temperature	↑	-	-	↑	↑	↑
Rainfall	↑	↑	↓	↑	↑↓	↑
Erosion	-	? ↑	↓	↓	↓	↓

of the secondary weathering products). The  $\delta^7Li$  of the bulk riverine solid load thus reflects weathering intensity but also the stoichiometry of the weathering reactions and the Li partition coefficient ( $K_{net}$ ) as well as the  $\delta^7Li$  of both the bedrock and the weathering products (cf. Dellinger et al., 2017).

The dependence of the solutions for dimensionless Li concentration (Li') and isotopic composition ( $\delta^7Li_r$ ) on the two dimensionless numbers ( $N_D^{Li}$  and  $K_{net}$ ) demonstrates that the Li systematics in river waters do not provide unique solutions for the multiple climatic and tectonic parameters that determine silicate chemical weathering fluxes. Table 2 speculates on some of the controls on the parameters comprising  $N_D^{Li}$  and  $K_{net}$  and illustrates the potential complexity of their interactions. For example, increases in rainfall may increase reaction rates, increasing the Damköhler number, but also increase fluid fluxes which has the opposite effect on  $N_D^{Li}$ . Increased rainfall may also increase erosion rates which would decrease weathering intensity but not chemical weathering fluxes. The relationship between erosion rate and the depth and length of groundwater flow paths in rapidly eroding mountainous terrains is unknown. Increases in temperature would increase reaction rates, increasing  $N_D^{Li}$ , but if the increase in temperature was associated with an increase in rainfall and erosion rate, this might offset the increase in reaction rate.

#### 7. Conclusions

Modelling of reactive transport along one-dimensional flow paths applicable to rapidly eroding catchments where weathering intensities are low shows that the controls on Li concentration and isotopic composition of river waters may be described by two dimensionless numbers; 1) a Damköhler number which is a product of reaction rate and water residence time and 2) a net partition coefficient that expresses the mass of Li in secondary minerals to the concentration of Li in the water from which the minerals are precipitating. The Li-isotopic composition of the river waters is controlled by the parameters that make up these dimensionless numbers including reaction rate, flow path length, fluid flux, Li fluid-solid partition coefficient and reaction stoichiometry, in addition to the Li content and isotopic composition of the bed rock. There is no simple relationship between weathering intensity and the Li-isotopic composition of the river waters. The Li-isotopic composition of solid weathering products does give a measure of weathering 'intensity', a measure of the fraction of silicate rock consumed by chemical weathering, but again is also a function of the other controlling parameters.

Analyses of Li concentrations and isotopic ratios of a set of major and minor rivers and bedload sediments from the headwaters of the Ganga river in the Himalayas illustrates how the reactive transport modelling may be applied to interpret the weathering environment. The results illustrate three contrasting weathering regimes. The output from the highest catchment on the Tibetan Sedimentary Series, which has the coldest climate and moderate erosion rates, displays lowest values of the net partition coefficient reflecting incipient weathering reactions

and/or low clay mineral/fluid partition coefficients. The high Li concentrations and relatively low  $\delta^7\text{Li}$  ratios in this catchment, plausibly a result of longer flow paths and lower fluid fluxes, dominate the Li-budget of the mainstem Alaknanda downstream. The most rapidly eroding High Himalayan Crystalline catchments are characterised by higher values of the net partition coefficient with water compositions tending towards the limiting isotopic fractionation of  $\sim +17\%$  expected at higher Damköhler numbers. The grouping of the waters along a relatively restricted range of net partition coefficient contours, but a wide range of Damköhler numbers, is consistent with relatively constant reaction stoichiometries but a wider range of fluid fluxes and/or flow path lengths. The lower altitude, warmer and more slowly eroding Lesser Himalayan catchments exhibit a more complex weathering environment. The high  $\delta^7\text{Li}$  ratios and lower Li concentrations of waters which exceed  $17\%$  can only be explained by a two stage weathering process where the second stage has a higher net partition coefficient than the first stage, so that the evolving water tends to lower Li concentrations but potentially much higher Li-isotopic ratios. This is plausibly the result of changing reaction stoichiometry along flow paths related to higher reaction progress in a more slowly eroding but faster chemical weathering environment.

The results illustrate how a set of geochemical and isotopic analyses may relate to the groundwater hydrology, climate, erosion rate, lithology and weathering reaction stoichiometries. Given the significance of rapidly eroding terrains for the potential climatic feedback of chemical weathering fluxes it will be essential to test whether the simple analysis of chemical weathering outputs, as modelled here, captures the important information or whether the additional potential complexities such as mixing of waters and progressive changes of reaction stoichiometries along flow paths obscure this information. The initial results from this study suggest that the modelling based on one-dimensional reactive transport equations with limited changes in reaction stoichiometry may provide valuable information on weathering regimes.

### Acknowledgements

James Bryson and Alex Morgan are thanked for helpful discussion. Iris van der Veen and Eric Deal are thanked for assistance in the field. We thank the editor Derek Vance, Philip Pogge von Strandmann and two anonymous reviewers for constructive comments which improved the manuscript. This project was supported in the framework of the Initial Training Network (ITN) iTECC funded by the EU REA under the FP7 implementation of the Marie Curie Action, under grant agreement number 316966, and NERC grant NE/P011659/1.

### Supplementary material

Supplementary material related to this article can be found as separate files BohlinBickle2019\_epsl\_supplementarytext and BohlinBickle2019\_epsl\_supplementarytables

### References

Andermann, C., Longuevergne, L., Bonnet, S., Crave, A., Davy, P., Gloaguen, R., 2012. Impact of transient groundwater storage on the discharge of Himalayan rivers. *Nature Geoscience* 5, 127-132.  
 Bagard, M.-L., West, A.J., Newman, K., Basu, A.R., 2015. Lithium isotope fractionation in the Ganges–Brahmaputra floodplain and implications for groundwater impact on seawater isotopic composition. *Earth and Planetary Science Letters* 432, 404-414.

Becker, J.A., Bickle, M.J., Galy, A., Holland, T.J.B., 2008. Himalayan metamorphic  $\text{CO}_2$  fluxes: Quantitative constraints from hydrothermal springs. *Earth and Planetary Science Letters* 265, 616–629.  
 Berner, R.A., Lasaga, A.C., Garrels, R.M., 1983. The carbonate-silicate geochemical cycle and its effect on atmospheric carbon dioxide over the past 100 million years. *American Journal of Science* 283, 641-683.  
 Bickle, M.J., 1992. Transport mechanisms by fluid-flow in metamorphic rocks: oxygen and strontium decoupling in the Trois Seigneurs massif - a consequence of kinetic dispersion? *American Journal of Science* 292, 289-316.  
 Bickle, M.J., Bunbury, J., Chapman, H.J., Harris, N.B., Fairchild, I.J., Ahmad, T., 2003. Fluxes of Sr into the headwaters of the Ganges. *Geochimica et Cosmochimica Acta* 67, 2567-2584.  
 Bickle, M.J., Chapman, H.J., Bunbury, J., Harris, N.B.W., Fairchild, I.J., Ahmad, T., Pomiès, C., 2005. The relative contributions of silicate and carbonate rocks to riverine Sr fluxes in the headwaters of the Ganges. *Geochimica et Cosmochimica Acta* 69, 2221–2240.  
 Bickle, M.J., Chapman, H.J., Tipper, E., De La Rocha, C.L., Ahmad, T., 2018. Chemical weathering outputs from the flood plain of the Ganga. *Geochimica et Cosmochimica Acta* 225, 146-175.  
 Bickle, M.J., Harris, N.B.W., Bunbury, J., Chapman, H.J., Fairchild, I.J., Ahmad, T., 2001. Controls on the  $^{87}\text{Sr}/^{86}\text{Sr}$  of carbonates in the Garwal Himalaya, headwaters of the Ganges. *J Geol* 109, 737-753.  
 Bickle, M.J., Tipper, E.D., Galy, A., Chapman, H.J., Harris, N.W.B., 2015. On discrimination between carbonate and silicate inputs to Himalayan rivers. *American Journal of Science* 315, 120-166.  
 Bluth, G., Kump, L., 1994. Lithologic and climatologic controls of river chemistry. *Geochim. Cosmochim. Acta* 58, 2341-2359.  
 Bohlin, M.S., Misra, S., Lloyd, N., Elderfield, H., Bickle, M.J., 2018. High precision determination of lithium and magnesium isotopes utilising single column separation and multi-collector inductively coupled mass spectrometry. *Rapid Communications In Mass Spectrometry* 32, 93-104.  
 Bookhagen, B., Burbank, D.W., 2010. Toward a complete Himalayan hydrological budget: Spatiotemporal distribution of snowmelt and rainfall and their impact on river discharge. *Journal of Geophysical Research* 115, F03019 03025 pp.  
 Bouchez, J., Von Blanckenburg, F., Schuessler, J.A., 2013. Modelling novel stable isotope ratios in the weathering zone. *American Journal of Science* 313, 267-308.  
 Calmels, D., Galy, A., Hovius, N., Bickle, M., West, A.J., Chen, M.C., Chapman, H., 2011. Contribution of deep groundwater to the weathering budget in a rapidly eroding mountain belt, Taiwan *Earth and Planetary Science Letters* 303, 48-58.  
 Chakrapani, G.J., Saini, R.K., 2009. Temporal and spatial variations in water discharge and sediment load in the Alaknanda and Bhagirathi Rivers in Himalaya, India. *Journal of Asian Earth Sciences* 35, 545-553.  
 Chamberlin, T.C., 1899. The influence of great epochs of limestone formation upon the constitution of the atmosphere. *J Geol* 6, 609-621.  
 Chan, L.H., Edmond, J.M., Thompson, G., Gillis, K., 1992. Lithium isotopic composition of submarine basalts: implications for the lithium cycle in the oceans. *Earth and Planetary Science Letters* 108, 151-160.  
 Coussens, J., Woodman, N., Upton, P., Menzies, C.D., Janku-Capova, L., Sutherland, R., Teagle, D.A.H., 2018. The significance of heat transport by shallow fluid flow at an active plate boundary: the Southern Alps, New Zealand. *Geophysical Research Letters* 45, 10,323–310,331.  
 Decarreau, A., Vigier, N., Palkova, H., Petit, S., Vieillard, P., Fontaine, C., 2012. Partitioning of lithium between smectite and solution: An experimental approach. *Geochimica et Cosmochimica Acta* 85, 314-325.  
 Dellinger, J., Bouchez, J., Gaillardet, J., Faure, L., Moureau, J., 2017. Tracing weathering regimes using the lithium isotope composition of detrital sediments. *Geology* 45, 411-414.  
 Dellinger, M., Gaillardet, J., Bouchez, J., Calmels, D., Louvat, P., Dosseto, A., Gorge, C., Alanoca, L., Maurice, L., 2015. Riverine Li isotope fractionation in the Amazon River basin controlled by the weathering regimes. *Geochimica et Cosmochimica Acta* 164, 71-93.

- Embersson, R., Hovius, N., Galy, G., Marc, O., 2016. Chemical weathering in active mountain belts controlled by stochastic bedrock landsliding. *Nature Geoscience* 9, 42-45.
- Evans, M.J., Derry, L.A., Anderson, S.P., France-Lanord, C., 2001. Hydrothermal source of radiogenic Sr to Himalayan rivers. *Geology* 29, 803-806.
- Fontorbe, G., De La Rocha, C.L., Chapman, H.J., Bickle, M.J., 2013. The silicon isotopic composition of the Ganges and its tributaries. *Earth and Planetary Science Letters* 381, 21-30.
- Gaillardet, J., Dupre, B., Louvat, P., Allegre, C.J., 1999. Global silicate weathering and CO<sub>2</sub> consumption rates deduced from the chemistry of large rivers. *Chemical Geology* 159, 3-30.
- Huh, Y., 2010. Estimation of atmospheric CO<sub>2</sub> uptake by silicate weathering in the Himalayas and the Tibetan Plateau: a review of existing fluvial geochemical data, in: Clift, P.D., Tada, R., Zheng, H. (Eds.), *Geological Society, London, Special Publications, London*, pp. 129-151.
- Huh, Y., Chan, L.-H., Zhang, L., Edmond, J.M., 1998. Lithium and its isotopes in major world rivers: implications for weathering and the oceanic budget. *Geochimica et Cosmochimica Acta* 62, 2039-2051.
- Kisakürek, B., James, R.H., Harris, N.B.W., 2005. Li and delta Li-7 in Himalayan rivers: Proxies for silicate weathering? *Earth and Planetary Science Letters* 237, 387-401.
- Lassey, K.R., Blattner, P., 1988. Kinetically controlled oxygen isotope exchange between fluid and rock in one-dimensional advective flow. *Geochimica et Cosmochimica Acta* 52, 2169-2175.
- Lemarchand, E., Chabaux, F., Vigier, N., Millot, R., Marie-Claire Pierret, M.-C., 2010. Lithium isotope systematics in a forested granitic catchment (Strengbach, Vosges Mountains, France). *Geochimica et Cosmochimica Acta* 74, 4612-4628.
- Lichtner, P.C., 1988. The quasi-stationary state approximation to coupled mass transport and fluid rock interaction in a porous medium. *Geochimica et Cosmochimica Acta* 52, 143-165.
- Liu, X.-M., Wanner, C., Rudnick, R.L., McDonough, W.F., 2015. Processes controlling  $\delta^7\text{Li}$  in rivers illuminated by study of streams and groundwaters draining basalts. *Earth and Planetary Science Letters* 409, 212-224.
- Lupker, M., Christian France-Lanord, C., Valier Galy, V., Lave, J., Gaillardet, J., Prasad Gajurel, A., Guilmette, C., Rahman, M., Kumar Singh, S., Sinha, R., 2012. Predominant floodplain over mountain weathering of Himalayan sediments (Ganga basin). *Geochimica et Cosmochimica Acta* 84, 410-432.
- Maher, K., 2010. The dependence of chemical weathering rates on fluid residence time. *Earth and Planetary Science Letters* 294, 101-110.
- Maher, K., 2011. The role of fluid residence time and topographic scales in determining chemical fluxes from landscapes. *Earth and Planetary Science Letters* 312, 48-58.
- Maher, K., Chamberlain, C.P., 2014. Hydrologic regulation of chemical weathering and the geologic carbon cycle. *Science* 343, 1502-1504.
- Maher, K., Steefel, C.I., White, A.F., Stonestrom, D.A., 2009. The role of reaction affinity and secondary minerals in regulating chemical weathering rates at the Santa Cruz Soil Chronosequence, California. *Geochimica et Cosmochimica Acta* 73, 2804-2831.
- Manaka, T., Araoka, D., Yoshimura, T., Hossain, H.M.Z., Nishio, Y., Suzuki, A., Kawahata, H., 2017. Downstream and seasonal changes of lithium isotope ratios in the Ganges-Brahmaputra river system. *Geochim. Geophys. Geosys.* 18, 3003-3015.
- Milliman, J.D., Meade, R.H., 1983. Worldwide delivery of river sediments to the oceans. *J Geol* 91, 1-19.
- Millot, R., Scaillet, B., Sanjuan, B., 2010a. Lithium isotopes in island arc geothermal systems: Guadeloupe, Martinique (French West Indies) and experimental approach. *Geochimica et Cosmochimica Acta* 74, 1852-1871.
- Millot, R., Vigier, N., Gaillardet, J., 2010b. Behaviour of lithium and its isotopes during weathering in the Mackenzie Basin, Canada. *Geochimica et Cosmochimica Acta* 74, 3897-3912.
- Misra, A., Froelich, P.N., (2012). Lithium isotope history of Cenozoic seawater: changes in silicate weathering and reverse weathering. *Science* 335, 818-823.
- Pistiner, J.S., Henderson, G.M., 2003. Lithium-isotope fractionation during continental weathering processes. *Earth and Planetary Science Letters* 214, 327-339.
- Pogge von Strandmann, P.A.E., Burton, K.W., Opfergelt, S., Eiríksdóttir, E.S., Murphy, M.J., Einarsson, A., Gislason, S.R., 2016. The effect of hydrothermal spring weathering processes and primary productivity on lithium isotopes: Lake Myvatn, Iceland. *Chemical Geology* 445, 4-13.
- Pogge von Strandmann, P.A.E., Frings, P.J., Murphy, M.J., 2017. Lithium isotope behaviour during weathering in the Ganges Alluvial Plain. *Geochimica et Cosmochimica Acta* 198, 17-31.
- Pogge von Strandmann, P.A.E., Porcelli, D., James, R.H., van Calsteren, P., Schaefer, B., Cartwright, I., Reynolds, B.C., Burton, K., 2014. Chemical weathering processes in the Great Artesian Basin: Evidence from lithium and silicon isotopes. *Earth and Planetary Science Letters* 406, 24-36.
- Singh, A.K., Hasnain, S.I., 1998. Major ion chemistry and weathering control in a high altitude basin: Alaknanda River, Garhwal Himalaya, India. *Hydrological Sciences Journal* 43, 825-843.
- Teng, F.-Z., McDonough, W. F., Rudnick, R. L., Dalpé, C., Tomascak, P. B., Chappell, B. W. and Gao, S. (2004) Lithium isotopic composition and concentration of the upper continental crust, *Geochimica et Cosmochimica Acta* 68, 4167-4178
- Tipper, E.T., Bickle, M.J., Galy, A., West, A.J., Pomie's, C., Chapman, H.J., 2006. The short term climatic sensitivity of carbonate and silicate weathering fluxes: Insight from seasonal variations in river chemistry. *Geochim. Cosmochim. Acta.* 70, 2737-2754.
- Valdiya, K.S., 1980. *Geology of Kumaun Lesser Himalaya*. Wadia Institute of Himalayan Geology, Dehra Dun.
- Vance, D., Bickle, M., Ivy-Ochs, S., Kubik, P.W., 2003. Erosion and exhumation in the Himalaya from cosmogenic isotope inventories of river sediments. *Earth and Planetary Science Letters* 206, 273-288.
- Verney-Carron, A., Vigier, N., Millot, R., 2011. Experimental determination of the role of diffusion on Li isotope fractionation during basaltic glass weathering. *Geochimica et Cosmochimica Acta* 75, 3452-3468.
- Vigier, N., Decarreau, A., Millot, R., Carignan, J., Petit, S., France-Lanord, C., 2008. Quantifying Li isotope fractionation during smectite formation and implications for the Li cycle. *Geochimica et Cosmochimica Acta* 72, 780-792.
- Walker, J.C.G., Hays, P.B., Kasting, J.F., 1981. A negative feedback mechanism for the long-term stabilisation of Earth's surface temperature. *Journal of Geophysical Research* 86, 9776-9782.
- Wanner, C., Bucher, K., Pogge von Strandmann, P.A.E., Waber, H.N., Pettke, T., 2017. On the use of Li isotopes as a proxy for water-rock interaction in fractured crystalline rocks: A case study from the Gotthard rail base tunnel. *Geochimica et Cosmochimica Acta* 198, 396-418.
- Wanner, C., Sonnenthal, E.L., Liu, X.-M., 2014. Seawater  $\delta^7\text{Li}$ : A direct proxy for global CO<sub>2</sub> consumption by continental silicate weathering? *Chemical Geology* 381, 154-167.
- West, A.J., Galy, A., Bickle, M., 2005. Tectonic and climatic controls on silicate weathering. *Earth and Planetary Science Letters* 235, 211-228.
- White, A. F. and Brantley, S. L. (2003) The effect of time on the weathering of silicate minerals: why do weathering rates differ in the laboratory and field? *Chemical Geology* 202, 479-506
- White, A.F., Schulz, M.S., Vivit, D.V., Blum, A.E., Stonestrom, D.A., Anderson, S.P., 2008. Chemical weathering of a marine terrace chronosequence, Santa Cruz, California I: Interpreting rates and controls based on soil concentration-depth profiles. *Geochimica et Cosmochimica Acta* 72, 36-68.
- Wimpenny, J., Gislason, S.R., James, R.H., Gannoun, A., Pogge Von Strandmann, P., Burton, K.W., 2010. The behaviour of Li and Mg isotopes during primary phase dissolution and secondary mineral formation in basalt. *Geochimica et Cosmochimica Acta* 74, 5259-5279.
- Zhang, L., Chan, L.-H., Gieskes, J.M., 1998. Lithium isotope geochemistry of pore waters from Ocean Drilling Program Sites 918 and 919, Irminger Basin. *Geochimica et Cosmochimica Acta* 62, 2437-2450.